Original Article

Imaging signs and the qualitative diagnosis of solitary rib lesions using ^{99m}technetium-methylene diphosphonate whole-body bone imaging in patients with a malignant tumor

Liang-Qian Tong[1#], Sheng-Nan Jiang[1#], Yan-Fang Sui[2], Yan-Hai Yin[3], Li-Qing Fu[1], Jiao-Yan Zhong[1], Jia-Ling Zhong[1]

[1]Department of Nuclear Medicine, Central South University Xiangya School Affiliated Haikou Hospital, Haikou, China; [2]Department of Rehabilitation Medicine, Central South University Xiangya School Affiliated Haikou Hospital, Haikou, China; [3]Department of Nuclear Medicine, Hainan Affiliated Hospital of Hainan Medicine University, Haikou, China

Contributions: (I) Conception and design: LQ Tong, YF Sui; (II) Administrative support: SN Jiang, YH Yin; (III) Provision of study materials or patients: SN Jiang, YH Yin; (IV) Collection and assembly of data: LQ Tong, LQ Fu, JY Zhong, JL Zhong; (V) Data analysis and interpretation: SN Jiang, YH Yin; (VI) Manuscript writing: All authors; (VII) Final approval of manuscript: All authors.

[#]The authors contributed equally to this work.

Correspondence to: Yan-Fang Sui, MM. Department of Rehabilitation Medicine, Central South University Xiangya School Affiliated Haikou Hospital, No. 43 Renmin Road, Meilan District, Haikou 570208, China. Email: suiyanfangsyf882@outlook.com; Yan-Hai Yin, MM. Department of Nuclear Medicine, Hainan Affiliated Hospital of Hainan Medicine University, No. 19 Xiuhua Road, Xiuying District, Haikou 570311, China. Email: yinyanhaiyyh85@outlook.com.

Background: The aim of this study was to summarize the valuable information for qualitative diagnosis by investigating the imaging signs from the whole-body bone imaging of solitary rib lesions.

Methods: A retrospective analysis was conducted of the data from 313 patients with malignant tumors and solitary rib lesions identified using whole-body bone imaging in Department of Nuclear Medicine of Central South University Xiangya School Affiliated Haikou Hospital between January 2015 and December 2017. Based on the final comprehensive diagnosis of the rib lesions, the patients were divided into a bone metastasis group, fracture group, other benign lesions group, and an uncertain group, and the characteristic imaging changes in rib lesions in each group were explored.

Results: (I) Significant differences were identified among the 4 groups (P<0.001) in the distribution of lesions in the anterior, posterior, and lateral ribs and proximal costal cartilage. The fracture group had the highest proportion of lesions in the anterior ribs (99/121, 81.8%) and proximal costal cartilage (74.4%, 90/121). (II) Significant differences were detected in morphology, concentration, boundaries, and radioactivity distribution among the 4 groups of patients (P<0.001). The bone metastasis group had the highest proportion of lesions appearing as stripes (35/67, 52.2%), and the fracture group had the highest proportion of lesions appearing as spots (94.2%, 114/121) and the lowest proportion appearing as stripes (3/121, 2.5%). (III) Significant differences were found in the longitudinal diameter, transverse diameter, aspect ratio, and tumor-to-normal tissue ratio between the 4 groups (P<0.001). The longitudinal diameter (27.8±16.0 mm) and aspect ratio (1.9±1.0) of the bone metastasis group were the highest, whereas the longitudinal diameter (15.2±3.9 mm) and aspect ratio (1.0±0.2) of the fracture group were the smallest.

Conclusions: This study revealed that different types of solitary rib lesions had relatively characteristic imaging signs in whole-body bone imaging.

Keywords: Rib; solitary; imaging signs; bone metastasis; whole-body bone imaging

Submitted Oct 24, 2022. Accepted for publication May 30, 2023. Published online Jul 24, 2023.
doi: 10.21037/qims-22-1159
View this article at: https://dx.doi.org/10.21037/qims-22-1159

Introduction

Bone is one of the organs in which the distant metastasis of many malignant tumors, such as advanced-stage lung cancer, most frequently occurs (1-3). The most common sites for the bone metastasis of malignant tumors are the spine, pelvis, and ribs. The ribs are flat bones with a rich blood supply, making them especially vulnerable to metastasis, with lung cancer, breast cancer, and prostate cancer—among other cancers—often metastasizing to the ribs (4-6). Imaging techniques for diagnosing bone metastases include X-ray, computed tomography (CT), magnetic resonance imaging, single-photon emission CT (SPECT), and positron emission tomography CT. Of the numerous techniques available, ^{99m}technetium-methylene diphosphonate (^{99m}Tc-MDP) whole-body bone imaging using SPECT is the simplest and most comprehensive screening method. Whole-body bone imaging has a high sensitivity for the detection of rib lesions, but it is difficult to qualitatively diagnose solitary rib lesions using this technique because of the flat imaging, low anatomical resolution, and non–tumor specific imaging agents. The typical manifestations of bone metastases in whole-body bone imaging are concentrated lesions on multiple bones of different sizes and shapes and a random distribution (7). However, in clinical application, whole-body bone imaging findings are often atypical, making qualitative diagnosis challenging. In addition, because of the large number of ribs, other benign lesions or injuries, such as fracture and bone island, can also easily occur (8). Whole-body bone imaging for patients with malignant tumors is mainly used to screen for bone metastasis. When solitary rib lesions are detected, the nature of the lesions directly affects the patient's treatment plan. Therefore, an accurate qualitative diagnosis is particularly important. At present, relatively few studies have been published on how to accurately diagnose solitary rib lesions. In clinical practice, we have found that the diagnosis of rib lesions is related to its location, morphology, and uptake, among other factors. Meanwhile, the tumor-to-normal tissue (T/N) ratio, aspect ratio, and other measurement indicators have been introduced to describe the lesions and are worth investigating. In this study, we retrospectively analyzed the data of 313 patients who had received a final diagnosis of a malignant tumor through pathology, with solitary rib lesions identified using whole-body bone imaging, to evaluate the imaging signs including location, morphology, uptake, radioactive distribution, boundaries, aspect ratio, and T/N ratio of the solitary rib lesions, thereby providing valuable information for qualitative diagnosis.

Methods

Demographics

A total of 313 patients (168 men and 145 women), aged 19–90 years (60.8±12.4 years), who had received a diagnosis of solitary rib lesions using whole-body bone imaging, had a history of malignant tumors, and had attended our department between January 2015 and December 2016 were included in the study. The medical history of all the patients was observed until December 2021. The inclusion criteria were as follows: (I) both a history of malignant tumors confirmed through pathology and (II) concurrent whole-body bone imaging revealing solitary rib lesions without other bone lesions. All whole-body bone imaging and chest–upper abdomen CT images, pathological diagnoses, and the medical records of the patients during the observation period were retrospectively analyzed using a picture archiving and communication system to make a final diagnosis of patients' rib lesions. Based on this final diagnosis, the patients were divided into 4 groups: a bone metastasis group (67 cases), fracture group (121 cases), other benign lesions group (118 cases), and uncertain group (7 cases). This study was conducted in accordance with the Declaration of Helsinki (as revised in 2013) and approved by the Ethics Committee of Central South University Xiangya School Affiliated Haikou Hospital (No. 2015-033). Informed consent was taken from all the patients.

The final diagnostic criteria for the rib lesions are listed below. (I) For bone metastasis, patients were required to meet 1 or more of 3 requirements: (i) a pathological diagnosis for rib lesions of metastasis, (ii) CT revealing obvious bone destruction in solitary rib lesions or bone destruction after a period of time, and (iii) whole-body bone imaging follow-up revealing enlarged rib lesions or lesions

not disappearing and new bone metastases appearing. (II) For fracture, the diagnostic criteria included CT uncovering indications such as continuity interruption, displacement, fracture line, callus formation, and fracture healing marks at the site of the rib lesions without bone destruction. (III) Other benign lesions were diagnosed if the lesions had disappeared in the absence of criteria 1 and 2 above after whole-body bone imaging or another imaging examination, and whole-body bone imaging follow-up showed that the lesions persisted, but CT revealed typical benign lesions (such as bone islands, bone cysts, and cord-like slightly high-density shadows) or negative manifestations. (IV) Uncertain lesions were those rib lesions that could not be diagnosed qualitatively by the existing clinical data within the observation time. Discordant results were resolved through joint reading.

Imaging method

Whole-body bone imaging was performed using American Infinia Hawkeye 4 SPECT (GE HealthCare), equipped with a low-energy and high-resolution parallel-hole collimator. All patients were intravenously injected with ^{99m}Tc-MDP (MDP kit supplied by Beijing Xinkesida Medicine, while the ^{99}Mo-^{99m}Tc generator was provided by Beijing HTA Co., Ltd., China; ^{99m}Tc-MDP radiochemical purity >95%) for 2–3 h at 370–740 MBq, and whole-body bone imaging (energy peak 140 keV, matrix 512×512, zoom 1.0) was then performed; the bladder was emptied and metal foreign bodies removed before imaging. The image was processed and analyzed using a Xeleris workstation (GE HealthCare), a nuclear medicine image processing system.

Image analysis and result determination

Two experienced nuclear medicine physicians jointly used the Xeleris workstation to analyze and evaluate the rib lesions from the whole-body bone imaging, recording the visual signs and measurement indicators to form the basis of the evaluation. Visual indicators mainly included (I) the location of the lesions (the left or right rib, the rib order number, the anterior/posterior/axillary rib, and proximity to the proximal costal cartilage); (II) focal morphology, including spots (the lesions did not obviously extend beyond the rib edge, and the longitudinal diameter of the rib was similar to the transverse diameter of the rib), stripes (the lesions formed stripes, and the longitudinal diameter was obviously greater than the transverse diameter), and other shapes (such as lumps and irregular shapes) (see *Figure 1*); (III) boundary clarity (clear, medium, or fuzzy); (IV) radioactivity distribution (even, medium, or uneven); and (V) concentration. With the spinal vertebral body, anterior superior iliac spine, and bladder of the normal ribs used as reference standards, the concentration of the lesions was classified into low-level uptake (the concentration was higher than that of the adjacent normal ribs and lower than that of the spinal vertebral body), medium-level uptake (the concentration was between that of the spinal vertebral body and anterior superior iliac spine), and high-level uptake (the concentration was higher than that of the anterior superior iliac spine or even higher than that of the bladder) (see *Figure 1*) (9). The measurement indices mainly included the aspect ratio of the lesion (the diameter of the lesion parallel to the ribs was taken as the longitudinal diameter, and the diameter of the lesion vertical to the ribs was taken as the transverse diameter, with the ratio of the two forming the aspect ratio) and T/N ratio (the ratio of maximum radioactive counts between the lesions and symmetric ribs with regions of interest of the same size).

Statistical analysis

SPSS 20.0 statistical software (IBM Corp.) was used for statistical analysis. The main measurement data are expressed as mean ± standard deviation ($\bar{x}$ ± s). A chi-squared test was used for intergroup comparisons of enumeration data, and a 1-way analysis of variance was used for intergroup comparisons of measurement data. A least significant difference (LSD) test was used for the posttest pairwise comparison. A binary logistic regression analysis was performed on the final diagnosis of bone metastasis or nonbone metastasis, fracture or nonfracture, and the presence of other benign lesions or absence of other benign lesions. $P<0.05$ indicated a statistically significant difference.

Results

Primary malignant tumors and rib lesions

Of the 313 patients included, there were 138 cases (44.0%) of lung cancer, 58 (18.5%) of breast cancer, 32 (10.2%) of nasopharyngeal cancer, 29 (9.2%) of prostate cancer, 13 (4.1%) of colorectal cancer, 9 (2.7%) of primary hepatocellular carcinoma, 8 (2.4%) of esophageal cancer, 7 (2.1%) of cervical cancer, 4 (1.2%) of thyroid cancer, and 4 (1.2%) of hypopharyngeal cancer. In addition, there

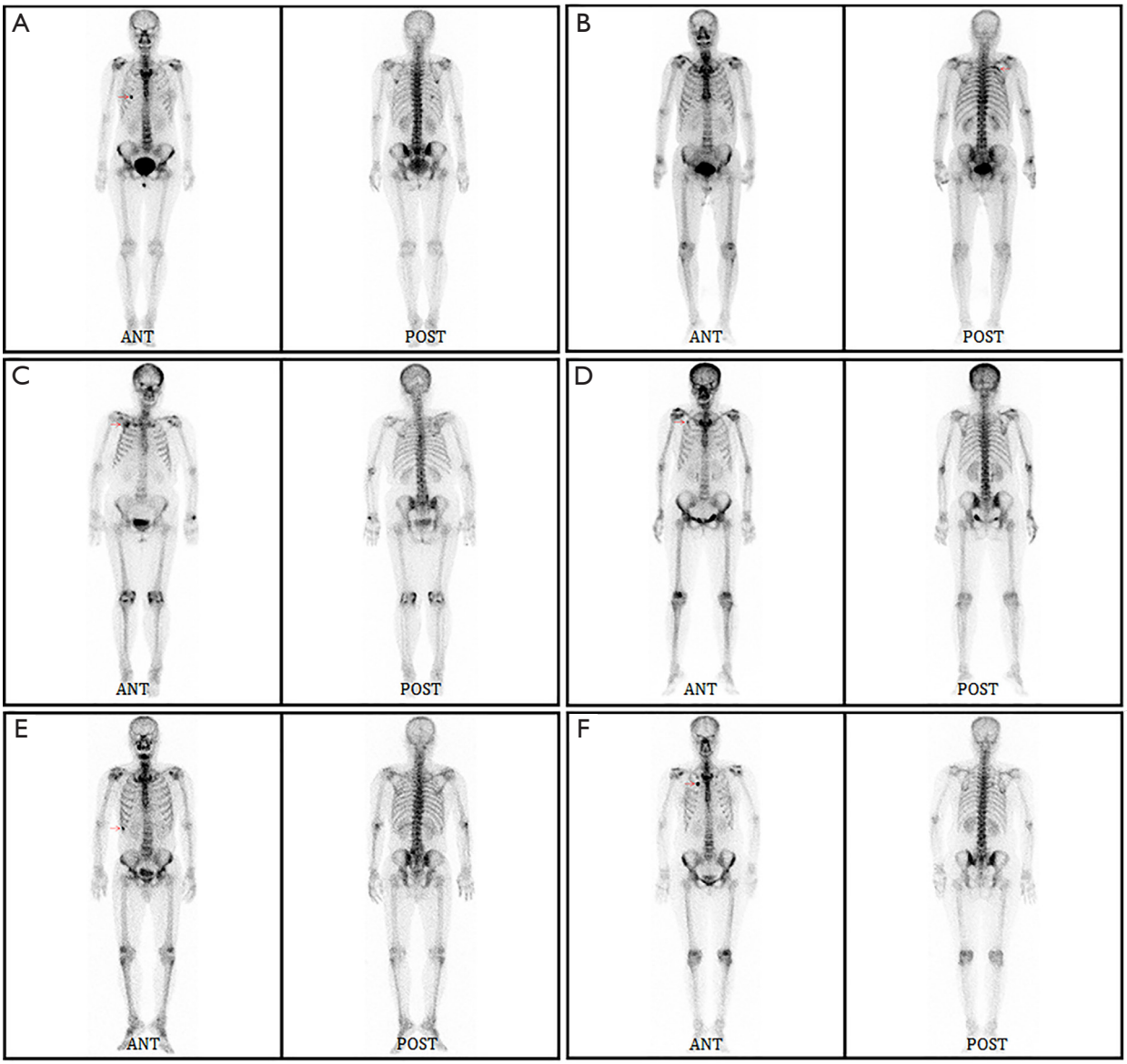

Figure 1 Example of morphology and concentration of solitary rib lesions. The rib lesion indicated by the arrow in (A) does not significantly extend beyond the rib edge, and the longitudinal diameter of the rib is similar to the transverse diameter of the rib. The morphology of the lesion is in the form of a spot. The longitudinal diameter of the rib lesion indicated by the arrow in (B) is obviously larger than the transverse diameter, appearing as a stripe. The rib lesion indicated by the arrow in (C) is irregular in shape and classified as "other shapes." The concentration of the rib lesion indicated by the arrow in (D) is greater than that of the adjacent normal ribs but lower than that of the sternal body; it is regarded as thin. The concentration of the rib lesion indicated by the arrow in (E) is higher than that of the sternal body but lower than that of the anterior superior spine; it is regarded as medium. The concentration of the rib lesion indicated by the arrow in panel 1f is higher than that of the anterior superior iliac spine and similar to the bladder concentration; it is regarded as dense. ANT, anterior; POST, posterior.

Table 1 Distribution of the solitary rib lesions in the left and right costae and anterior and posterior axillary costae, and whether they were near the costal cartilage end

Lesion location	Bone metastasis group (n=67)	Fracture group (n=121)	Other benign lesion group (n=118)	Uncertainty group (n=7)	χ^2	P
Bilateral rib						
Left side	23 (34.3%)	55 (45.5%)	57 (48.3%)	1 (14.3%)	6.022	0.111
Right side	44 (65.7%)	66 (54.5%)	61 (51.7%)	6 (85.7%)		
Anterior/posterior/axillary						
Anterior rib	25 (37.3%)	99 (81.8%)	54 (45.8%)	1 (14.3%)	59.851	< 0.001
Posterior rib	35 (52.3%)	11 (9.1%)	43 (36.4%)	4 (57.1%)		
Axillary lateral ribs	7 (10.4%)	11 (9.1%)	21 (17.8%)	2 (28.6%)		
Proximal costal cartilage end						
Yes	13 (19.4%)	90 (74.4%)	38 (32.2%)	0 (0)	73.458	<0.001
No	54 (80.6%)	31 (25.6%)	80 (67.8%)	7 (100.0%)		

The proportion of rib lesion located on the right rib side in the bone metastasis group was higher (about 65.7%), but no significant difference was found compared with the fracture group and the other benign lesion group (χ^2=2.199, P=0.138; χ^2=3.401, P=0.065), and there was no significant difference between the fracture group and the other benign lesion groups (χ^2=0.195, P=0.659). The anterior rib distribution of the fracture group was as high as 81.8%, which was significantly higher than that in the bone metastasis group and the other benign lesion group (χ^2=45.844, P<0.001; χ^2=35.291, P<0.001), and no significant difference was found in the anterior/posterior/axillary rib distribution between the bone metastasis group and the other benign lesion group (χ^2=4.769, P=0.092). The proportion of lesion located near costal cartilage in the fracture group was as high as 74.4%, which was significantly higher than that in the bone metastasis group and the other benign lesion group (χ^2=52.617, P<0.001; χ^2=42.725, P<0.001), but the bone metastasis group and the other benign lesion group showed no significant difference in whether the lesion was located in the proximal costal cartilage (χ^2=3.507, P=0.061, >0.05).

were 4 cases of lymphoma (1.2%), 3 (0.9%) of gastric-duodenal cancer, 1 (0.3%) of bladder cancer, 1 (0.3%) of tongue cancer, 1 (0.3%) of gingival cancer, and 1 (0.3%) of endometrial cancer. The final diagnosis rates of the solitary rib lesions, bone metastasis, and other benign lesions were 21.4% (67/313), 38.7% (121/313), and 37.7% (118/313), respectively; 7 cases (2.2%) could not be diagnosed qualitatively. For the whole-body bone imaging of all 313 patients, the diagnostic coincidence rate was 69.6%, and the misdiagnosis rate was 30.4%. Among the top 4 malignant tumors with the highest incidence of solitary rib lesions, including lung cancer (138 cases), breast cancer (58 cases), nasopharyngeal cancer (32 cases) and prostate cancer (29 cases), there was no significant difference (P>0.05) in the location of the solitary rib lesions.

Location of the solitary rib lesions

Regarding the location of the lesions, there were 136 (43.4%) on the left rib and 177 (56.6%) on the right rib; 179 (57.2%) on the anterior ribs, 93 (29.7%) on the posterior ribs, and 41 (13.1%) on the axillary ribs; 141 (45.0%) near the proximal costal cartilage, and 172 (55.0%) not near the proximal costal cartilage. The distribution of the rib lesions in the 2^{nd}–10^{th} ribs in the bone metastasis group tended to be balanced, and the distribution of rib lesions in the 1^{st}–12^{th} ribs in the fracture group and other benign lesions group presented a left-skewed distribution and right-skewed distribution, respectively, but the chi-squared test indicated there to be no difference among the 3 groups (P>0.05). The number of patients in the uncertain group was small, and the distribution characteristics of lesions on the 1^{st}–12^{th} ribs were unclear (see *Table 1* and *Figure 2* for the specific distribution).

Visual parameters, including shape, concentration, boundaries, and radioactive distribution of the solitary rib lesions

(I) The percentage of rib lesions in the bone metastasis

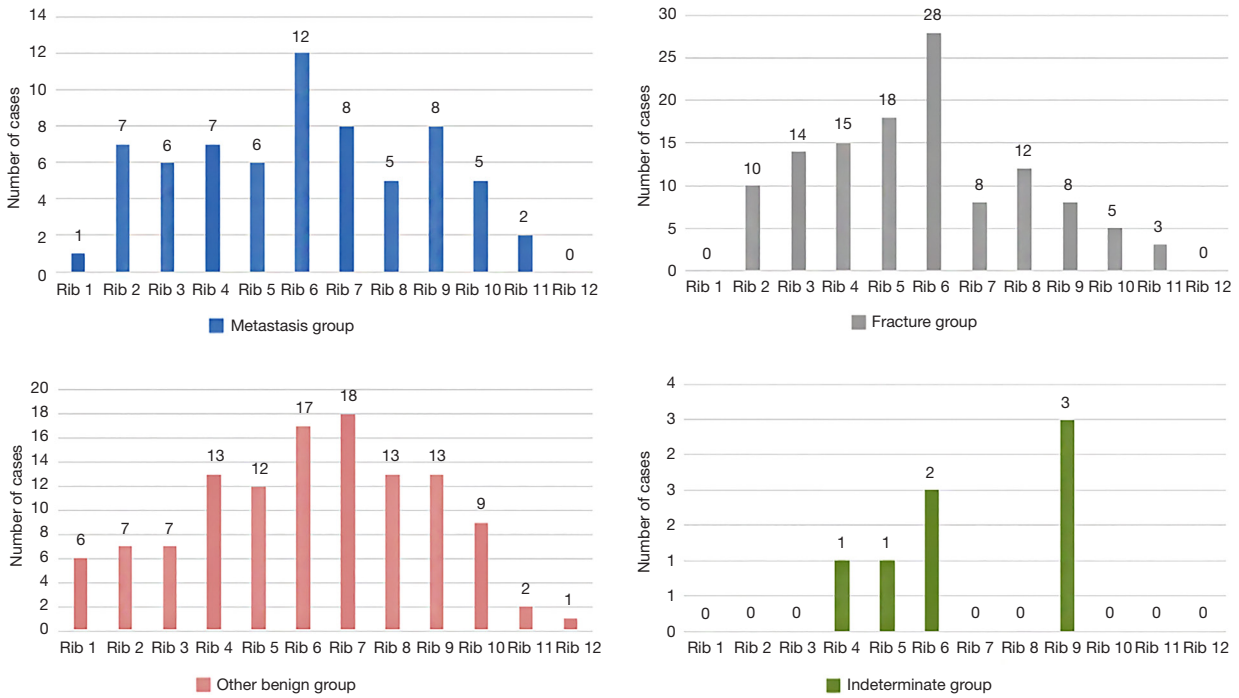

Figure 2 Distribution of solitary rib lesions on the 1st–12th ribs.

group that appeared as stripes was 52.2%, which was significantly higher than that of the fracture and other benign lesions groups. Most of the lesions in the fracture group were in the form of spots (approximately 94.2%), with few stripes or other shapes (approximately 2.5% and 3.3%, respectively). A significant difference was detected in lesion morphology between the bone metastasis, fracture, and other benign lesions groups (${}^{MF}\chi^2$=73.189, ^{MF}P<0.001; ${}^{MB}\chi^2$=24.795, ^{MB}P<0.001; ${}^{FB}\chi^2$=19.085, ^{FB}P<0.001). (II) The fracture group had the highest proportion of densely concentrated rib lesions (up to 66.1%), and the other benign lesions group had the highest proportion of thinly concentrated rib lesions (56.8%); the bone metastasis and fracture groups had a relatively low proportion of thinly concentrated rib lesions (13.4% and 12.4%, respectively). A significant difference was detected in the concentration of lesions between the bone metastasis, fracture, and other benign lesions groups (${}^{MF}\chi^2$=7.151, ^{MF}P=0.028<0.05; ${}^{MB}\chi^2$=33.381, ^{MB}P<0.001; ${}^{FB}\chi^2$=60.477, ^{FB}P<0.001). (III) The proportion of clear rib lesion boundaries in the fracture group was 71.8%, which was much higher than that of other groups. The proportion of fuzzy rib lesion boundaries in the other benign lesions group was 46.6%, which was higher than that of the bone metastasis and fracture groups. Significant differences were identified in the degree of clear rib lesion boundaries between the bone metastasis, fracture, and other benign lesions groups (${}^{MF}\chi^2$=16.321, ^{MF}P<0.001; ${}^{MB}\chi^2$=12.707, ^{MB}P=0.002<0.01; ${}^{FB}\chi^2$=52.915, ^{FB}P<0.001). (IV) The proportion of uneven radiation distribution among rib lesions in the bone metastasis group was higher than that of the other groups (up to 32.8%), and most of the lesions in the fracture and other benign lesions groups exhibited uniform radiation distribution, with proportions of 86.8% and 71.2%, respectively. Significant differences were detected in the radiation distribution of rib lesions between the bone metastasis, fracture, and other benign lesions groups (${}^{MF}\chi^2$=40.730, ^{MF}P<0.001; ${}^{MB}\chi^2$=13.472, ^{MB}P=0.001<0.01; ${}^{FB}\chi^2$=10.246, ^{FB}P=0.006<0.01; see *Table 2* for details).

Quantitative parameter analysis of solitary rib lesions

A postmortem comparison (LSD) revealed that the longitudinal diameter of solitary rib lesions in the bone metastasis group was significantly larger than that of the fracture and other benign lesions groups (P<0.001), and the longitudinal diameter in the fracture group was the smallest and was significantly different from that of the

Table 2 Visual parameters including shape, concentration degree, boundary, and radioactive distribution of solitary rib lesions

Visual parameters	Bone metastasis group (n=67)	Fracture group (n=121)	Other benign lesion group (n=118)	Uncertainty group (n=7)	χ^2	P
Form						
Spot shape	26 (38.8%)	114 (94.2%)	88 (74.6%)	4 (57.1%)	76.187	<0.001
Strip shape	35 (52.2%)	3 (2.5%)	22 (18.6%)	3 (42.9%)		
Other shapes	6 (9.0%)	4 (3.3%)	8 (6.8%)	0 (0)		
Degree of concentration						
Thick	32 (47.8%)	80 (66.1%)	26 (22.0%)	0 (0)	84.692	<0.001
Medium	26 (38.8%)	26 (21.5%)	25 (21.2%)	3 (42.9%)		
Thin	9 (13.4%)	15 (12.4%)	67 (56.8%)	4 (57.1%)		
Borderline						
Clear	29 (43.3%)	87 (71.8%)	30 (25.4%)	0 (0)	67.346	<0.001
Medium	24 (35.8%)	17 (14.1%)	33 (28.0%)	3 (42.9%)		
Fuzzy	14 (20.9%)	17 (14.1%)	55 (46.6%)	4 (57.1%)		
Radioactive distribution						
Even	31 (46.3%)	105 (86.8%)	84 (71.2%)	3 (42.8%)	43.926	<0.001
Medium	14 (20.9%)	12 (9.9%)	19 (16.1%)	2 (28.6%)		
Uneven	22 (32.8%)	4 (3.3%)	15 (12.7%)	2 (28.6%)		

other benign lesions group (P=0.026, <0.05). There were no significant differences in the transverse diameter of rib lesions between the bone metastasis and fracture groups (P=0.672, >0.05), but the transverse diameter in the other benign lesions group was smaller than that in the bone metastasis and fracture groups, and the difference was significant (^{MB}P=0.002, <0.01; ^{FB}P<0.001). The aspect ratio of the bone metastasis group was higher than that of the fracture and other benign lesions groups (P<0.001), and the aspect ratio of the other benign lesions group was higher than that of the fracture group (P<0.001); thus, the bone metastasis lesions tended to appear as stripes. The T/N ratio in the fracture group was the highest, followed by that in the bone metastasis group, but it was relatively low in the other benign lesions group; thus, in general, the concentration of solitary rib lesions caused by fracture was relatively high, that of bone metastases was medium, and that of other benign lesions was relatively low (^{MF}P=0.021, <0.05; ^{MB}P<0.001; ^{FB}P<0.001).

Logistic regression analysis of bone metastasis, fracture, and other benign lesions

Based on the final diagnosis, 313 patients were divided into bone metastasis and nonbone metastasis, fracture and nonfracture, and presence of benign lesions and absence of other benign lesions groups, and a binary logistic regression analysis was performed. Five parameters (proximity of the rib lesions to the proximal costal cartilage, shape, concentration, aspect ratio, and T/N ratio) were significant for the diagnosis of bone metastasis (P=0.001, P=0.011, P=0.009, P=0.015, and P=0.048, respectively; see *Table 3* for details). Meanwhile, the significant factors for the diagnosis of fracture included patient's age; lesion distribution on the anterior, posterior, and axillary ribs; proximity to the proximal costal cartilage; concentration; and T/N ratio (P=0.021, P=0.038, P=0.004, P=0.021, and P=0.008, respectively; see *Table 3* for details). The boundary and concentration parameters were significant for the diagnosis

Table 3 Factorial analysis and binomial logistic regression analysis on bone metastasis, fracture and other benign lesions

Item	Bone metastasis and nonbone metastasis			Fracture and nonfracture			Other benign lesions and no other benign lesions		
	B value	Wald	P value	B value	Wald	P value	B value	Wald	P value
Gender	–0.163	0.232	0.63	–0.476	2.261	0.133	0.094	0.108	0.742
Age	0.103	0.138	0.71	–0.644	5.294	0.021	0.436	3.838	0.066
Left/right rib	–0.566	2.735	0.098	0.313	0.996	0.318	0.222	0.642	0.423
Rib sequence number	0.015	0.046	0.830	–0.029	0.203	0.652	0.004	0.005	0.944
Anterior/posterior/axillary rib	0.057	0.040	0.842	–0.505	0.284	0.038	0.068	0.073	0.787
Proximal costal cartilage end	–1.534	10.753	0.001	1.182	8.377	0.004	–0.171	0.189	0.664
Form	–0.719	0.282	0.011	–0.174	0.396	0.529	–0.014	0.004	0.947
Borderline	–0.053	0.021	0.885	0.050	0.018	0.893	0.707	6.005	0.014
Radioactive distribution	–0.423	3.000	0.083	–0.035	0.014	0.905	0.319	2.010	0.156
Degree of concentration	0.956	6.896	0.009	0.644	5.294	0.021	–0.879	8.727	0.003
Longitudinal diameter	–0.027	0.226	0.634	0.080	0.497	0.481	–0.021	0.165	0.685
Transverse diameter	–0.012	0.016	0.901	0.020	0.025	0.875	0.085	0.960	0.327
Aspect ratio	0.872	5.929	0.015	0.973	0.344	0.558	0.316	0.175	0.676
T/N ratio	0.125	0.499	0.048	–0.475	6.976	0.008	0.316	2.754	0.097
Constant	4.674	5.363	0.021	–1.540	0.395	0.53	–2.670	2.165	0.141

Binary logistic regression analysis was performed on factors of bone metastasis and nonbone metastasis, fracture and nonfracture, and other benign lesions and no other benign lesions respectively. Age stratification: ≤40, >40–60, and >60 years old. T/N ratio, tumor-to-normal tissue ratio.

of other benign lesions (P=0.014 and P=0.003, respectively; see *Table 3* for details). Bone metastatic lesions were rarely detected near the proximal costal cartilage and had a higher proportion with a striped morphology, medium concentration of lesions, large aspect ratio, and medium T/N ratio. Patients over 60 years were more likely to have fractures, and the proportion of fractures in patients below the age of 40 years was small (1 case in the group). The proportion of fracture lesions located at the anterior rib and near the proximal costal cartilage was significantly large, and the concentration of fracture lesions and T/N ratio was significantly high.

Discussion

The typical manifestation of multiple bone metastases from malignant tumors in whole-body bone imaging is as multiple randomly distributed lesions of different sizes, shapes, and concentrations, which makes diagnosis easier. However, currently, patients are often discovered with tumors at an advanced stage, and thus the optimal treatment time is often missed (10). Whole-body bone imaging has a high sensitivity for the detection of bone metastases. The early diagnosis and treatment of bone metastases in a small single lesion can effectively delay progression, improving survival time and the quality of life. The misdiagnosis of benign solitary rib lesions as bone metastasis when using whole-body bone imaging leads to overtreatment, whereas the misdiagnosis of bone metastasis as benign lesions delays treatment. Many malignant tumors are prone to rib metastasis, which can be easily detected through whole-body bone imaging, but only some solitary rib lesions are bone metastasis. In this study, bone metastatic lesions accounted for approximately 21.4% (67/313) of the lesions analyzed, and the majority were fractures (121/313, 38.7%) and other benign lesions (118/313, 37.7%). Among the 313 patients, the 4 tumor types with the highest incidence of rib metastasis were lung cancer (38/138, 27.5%), prostate cancer (6/29, 20.7%), nasopharyngeal carcinoma (6/32, 18.8%), and breast cancer (9/58, 15.5%). An

epidemiological study of a group of 1,672 patients with prostate cancer in Beijing revealed that the proportion of bone metastasis in patients with prostate cancer was very high, reaching 44.1% (737/1,672) (11).

Whole-body bone imaging uses plane imaging, but this provides an unclear anatomical structure, possesses few diagnostic dimensions, and has a limited literature on the related imaging signs. No guidelines appear to exist for the qualitative diagnosis of solitary rib lesions. Li *et al.* (12) summarized and analyzed the data of 613 patients with breast cancer with bone scan abnormalities and found that there were as many as 324 cases with rib abnormalities (approximately 52.9%), but the proportion of bone metastasis was very low (only 1.2%) in patients with only rib lesions in bone imaging, and the proportion of bone metastasis was very high (reaching 51.0%) when there were multiple rib lesions or lesions coexisting in the ribs and other bones. Therefore, multiple rib lesions or their combination with other bone lesions can be helpful for diagnosing rib metastasis. Li *et al.*'s study mainly focused on the significance of the number of rib lesions and their confusion with other bone lesions when identifying rib metastases; it did not focus on the imaging signs (location, shape, radiation distribution, boundaries, concentration, etc.) of the lesions.

The present study mainly explored the imaging signs of rib lesions. We found that rib fractures were more likely to be located in the anterior rib and mostly near the proximal costal cartilage, accounting for 81.8% and 74.4%, respectively (see *Table 1*). The location preference of rib fractures is significant and is greatly helpful for diagnosis. This may be because anterior ribs have a larger range of motion, and their covering muscles are weaker than those of the posterior and axillary ribs. The primary reason for fractures to occur easily near the proximal costal cartilage is that it is anatomically a transitional zone, being less firm than the rib–costal cartilage junction and the distal costal cartilage. It is worth noting that in this study, no fracture was detected at the proximal costal cartilage or the rib–costal cartilage junction. The distribution in the bone metastasis and other benign lesions groups at the anterior, posterior, and axillary ribs had no significant characteristics, but it is worth mentioning that some bone metastases and other benign lesions were located at the proximal costal cartilage, accounting for 19.4% in the bone metastasis group and 32.2% in the other benign lesion group, respectively (see *Table 1*); this proportion is much lower than that in the fracture group. The distribution of rib lesions in the bone metastasis group in the 2^{nd}–10^{th} ribs was relatively balanced, which was consistent with the random distribution in the bone metastasis group. The distribution in the 1^{st}–12^{th} ribs in the fracture and other benign lesions groups was essentially normal. However, there was no significant difference in distribution between the 3 groups, which might be related to the small number of cases.

Based on the final diagnosis of rib lesions, patients were divided into a bone metastasis group, fracture group, other benign lesions group, and uncertain group. We found that the whole-body bone imaging signs of rib lesions were distinct for each group. Rib metastatic lesions often broke through the rib cortex and progressed along the longitudinal diameter of ribs. The longitudinal diameter of the lesions was longer, their transverse diameter was close to or larger than that of the ribs, and the average aspect ratio was 1.9 (see *Figure 3*). Therefore, the whole-body bone images often appeared as stripes. The suture ran vertically or nearly vertically through the ribs and rarely extended along the longitudinal diameter of the ribs. During the repair period, a callus formed to wrap around the fracture suture; therefore, the lesion morphology was mostly pointed and rarely striped, the longitudinal diameter was close to or even slightly shorter than the transverse diameter, and the average aspect ratio was 1.0 (see *Figure 3*). Other benign lesions (such as bony islands or high-density shadows in the bone marrow cavity) were mostly located in the ribs; their transverse diameter was therefore often small (often smaller than that of the ribs), with an average aspect ratio of 1.4 (see *Figure 3*). The fracture lesions were highly concentrated, with a clear boundary and uniform radioactivity distribution. In this study, the proportions of the concentrated lesions, clear boundaries, and uniform radioactivity distribution in the fracture group were 66.1%, 71.8% and 86.8%, respectively, and the T/N ratio was as high as 3.1±1.5. All the above indicators were significantly higher than those of the other 3 groups (all P values <0.001). This may be related to the rich blood supply and extremely active bone metabolism near the fracture line in the fracture healing stage. Concurrent CT scans often revealed clear fracture lines and callus formation. The concentrations of radioactivity in most of the bone metastatic lesions were of medium thickness, and the proportion of boundaries with medium-level blurring increased. For the bone metastasis group, the proportion of uneven radioactivity distribution was the largest (32.8%),

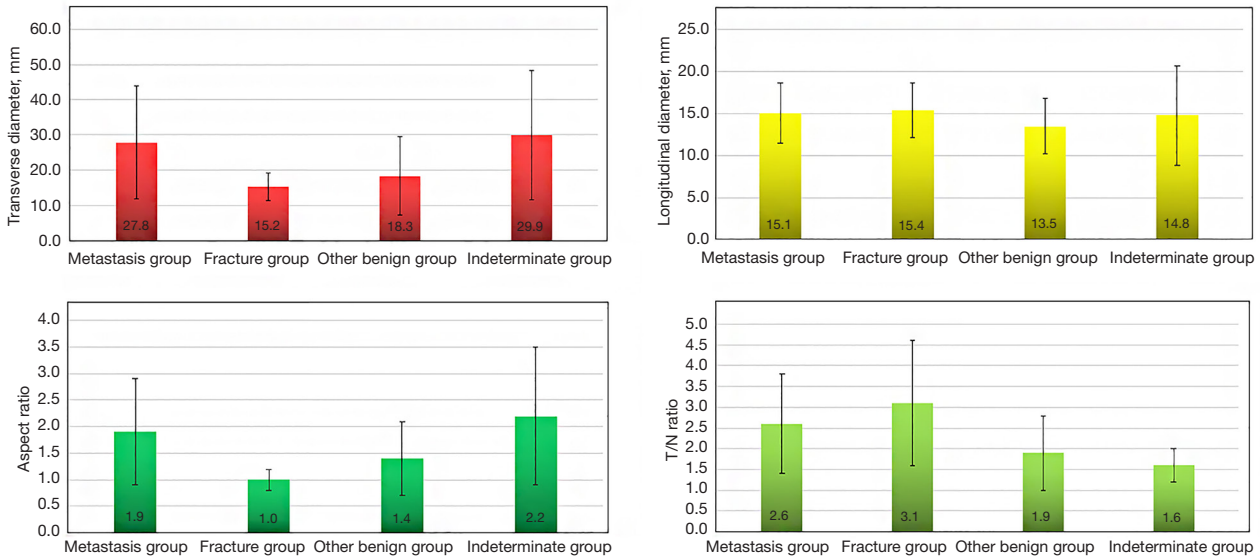

Figure 3 Quantitative parameter analysis of solitary rib lesions. Significant differences were identified in the longitudinal diameter, transverse diameter, aspect ratio, and tumor-to-normal tissue (T/N) ratio ($F_{\text{longitudinal diameter}}$ =22.903, $P_{\text{longitudinal diameter}}$ <0.001; $F_{\text{transverse diameter}}$ =6.661, $P_{\text{transverse diameter}}$ <0.001; $F_{\text{aspect ratio}}$ =26.113, $P_{\text{aspect ratio}}$ <0.001; $F_{T/N}$ =26.113, $P_{T/N}$ <0.001).

and the T/N ratio of the metastasis group (2.6±1.2) was lower than that of the fracture group (3.1±1.5). This may be because bone metastases can be osteogenic, osteoclastic, or both, and active osteogenic and osteoclastic activities coexist in most cases. A variety of other benign rib lesions exist, and it is difficult to characterize the specific disease. In this study, we noted that other isolated benign rib lesions often presented as spots (74.6%) and had a weak concentration (56.8%), fuzzy boundaries (46.6%), uniform radioactivity distribution (71.2%), and the smallest T/N ratio (1.9±0.9) in whole-body bone imaging. At present, when nuclear medicine physicians use whole-body bone imaging to form diagnoses, the resolution of the lesion from normal bone and the qualitative diagnosis of lesions are mainly based on a visual assessment (13). Therefore, the process of analyzing the visual imaging signs from whole-body bone imaging forms the basis of the diagnosis.

In this study, based on the whole-body bone imaging of all the patients, when the lesions appeared as stripes and the radioactive distribution was uneven, the proportion of bone metastasis was the highest (stripes: 35/63, 55.6%; uneven distribution: 22/43, 51.2%). Therefore, striped lesions and an uneven radioactivity distribution were the imaging manifestations typical of bone metastasis. However, in the logistic regression analysis bone metastasis was not significantly associated (P=0.083, >0.05) with the distribution of radioactivity. This study also revealed that in whole-body bone imaging, the fracture lesion near the proximal costal cartilage was located at the rib–costal cartilage junction, but in the CT scans, the fracture was not located at the rib–costal cartilage junction but 1–2 cm away from this junction. This might be because it was one of the smaller extensions of the enlarged costal cartilage, such as the femoral neck, that was prone to fractures (see *Figure 4*).

There are still some limitations in this study. First, the number of cases was small, and morphology and aspect ratio interfered with each other as did concentration and T/N ratio. Therefore, the results of the factorial analysis and chi-squared test were not consistent. Second, only a few of the patients included in this study underwent SPECT/CT tomography. SPECT/CT is especially equipped with specific quantitative devices that can help characterize this type of lesion. SPECT/CT fusion imaging can improve sensitivity and specificity by reducing ambiguous interpretation as compared to planar imaging or SPECT alone. Therefore, studies based on larger sample sizes and comparison of different examination methods are still necessary.

Conclusions

To our knowledge, this is the first study to comprehensively

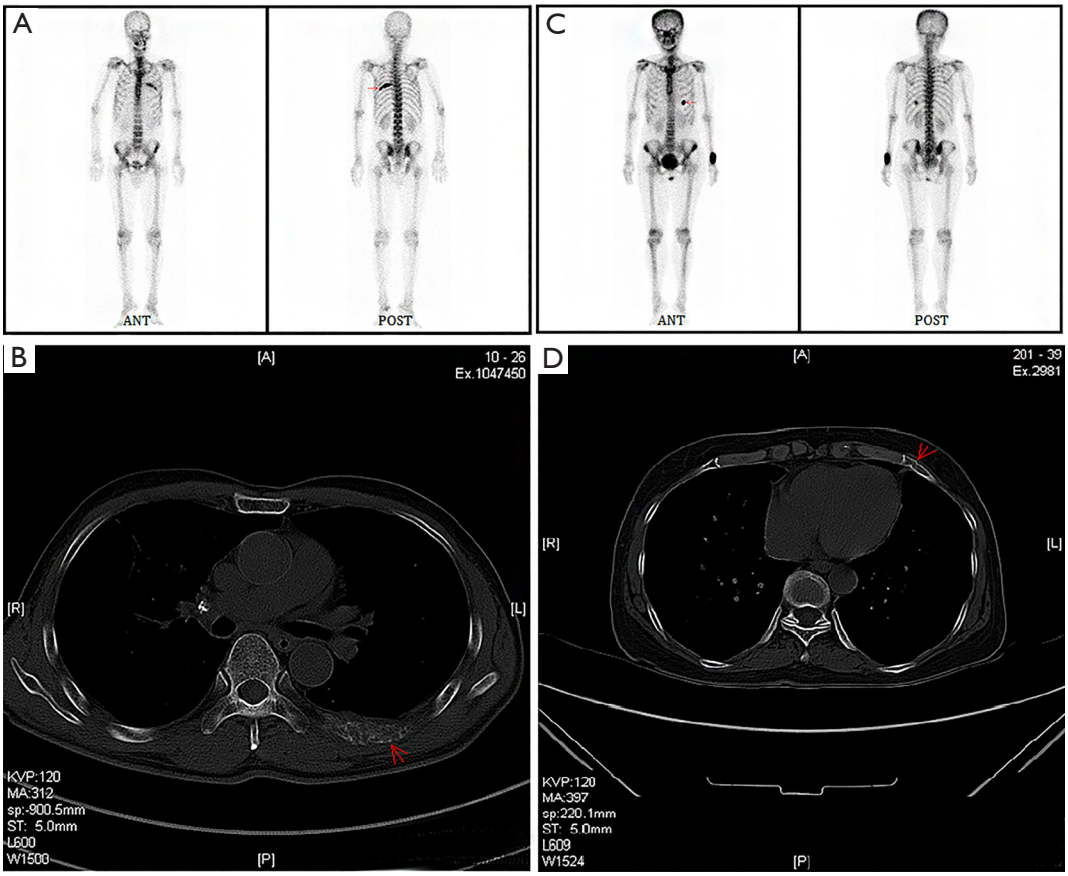

Figure 4 Whole-body bone imaging (A,C) and computed tomography (B,D) imaging findings of rib striped lesions and the proximal costal cartilage. In (A), the solitary rib lesions in the left seventh posterior rib (red arrow) appear as stripes with uneven radioactivity distribution, whereas in (B), the destruction of the left seventh posterior rib (red arrow) is clear, with coexisting osteogenesis and osteoclast. Bone metastasis is diagnosed. In (C), the solitary rib lesions of the left 6th anterior rib (red arrow) are located near the proximal costal cartilage, appearing as a spot; it is thick and has a clear boundary. In (D), the fracture line has a slight dislocation at the fracture site and a small amount of callus formation at the extension of the proximal costal cartilage of the left sixth anterior rib (red arrow); it is diagnosed as fracture.

explore the imaging features of solitary rib lesions with different properties in the whole-body bone imaging of patients with malignant tumors. Our research reported that one-fifth (21.4%) of the solitary rib lesions in these patients were bone metastases, with most identified as fractures (38.7%) or other benign lesions (37.7%). Moreover, in our study, solitary rib lesions with different characteristics had distinct imaging signs in whole-body bone imaging. Characteristic imaging signs of bone metastatic lesions included random locations on the anterior, posterior, axillary rib, and 1st–12th ribs, striped morphology, and uneven radioactivity distribution. Patients with fracture were usually older, and the fracture lesions mostly located in the anterior rib, especially near the proximal costal cartilage, were more likely to appear as spots than as stripes and had markedly strong radioactivity and clear boundaries. Other benign lesions were mostly pale punctiform lesions with unclear borders. These findings provide valuable information for diagnosis by nuclear medicine physicians (see *Figure 5*). However, some imaging signs of the solitary rib lesions of bone metastasis, fracture, and other benign lesions through whole-body bone imaging overlap and are not typical; therefore, the characteristic imaging signs should be identified and verified in a larger sample size and

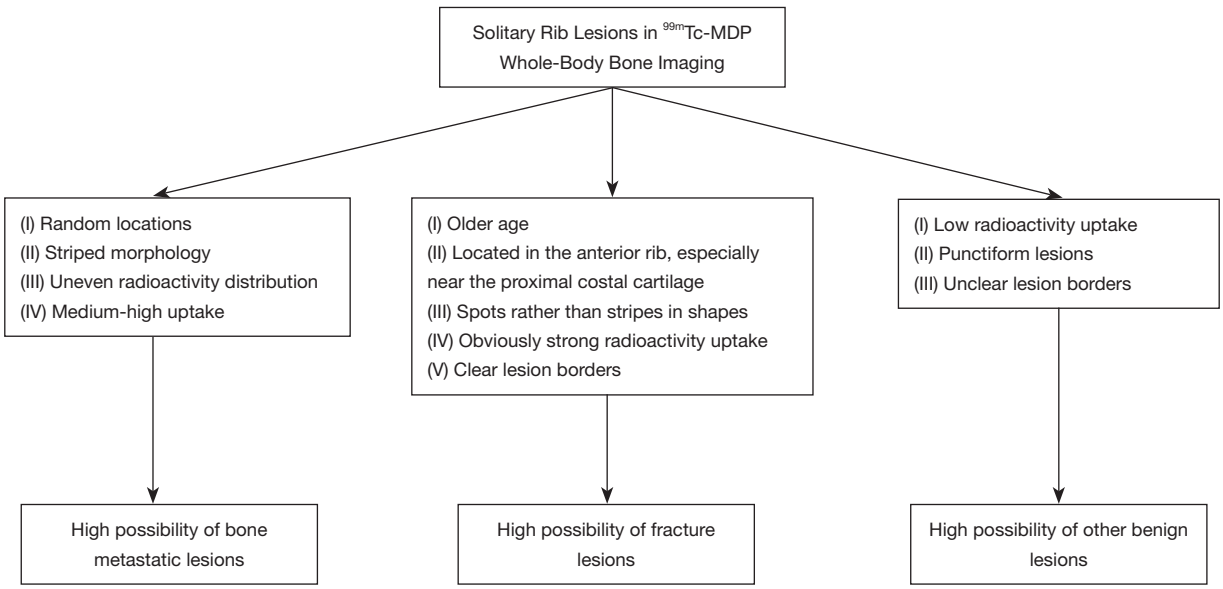

Figure 5 Diagnostic flowchart for solitary rib lesions in ^{99m}Tc-MDP whole-body bone imaging. ^{99m}Tc-MDP, ^{99m}technetium-labeled methylene diphosphonate.

through multicenter clinical research.

Acknowledgments

We would like to acknowledge the hard and dedicated work of all the staff that implemented the intervention and evaluation components of the study.
Funding: This study was supported by the Healthy Department of Hainan Province Foundation (No. 21A200039) and Hainan Province Clinical Medical Center (No. 0202067).

Footnote

Conflicts of Interest: All authors have completed the ICMJE uniform disclosure form (available at https://qims.amegroups.com/article/view/10.21037/qims-22-1159/coif). The authors have no conflicts of interest to declare.

Ethical Statement: The authors are accountable for all aspects of the work in ensuring that questions related to the accuracy or integrity of any part of the work are appropriately investigated and resolved. This study was conducted in accordance with the Declaration of Helsinki (as revised in 2013) and approved by the Ethics Committee of Central South University Xiangya School Affiliated Haikou Hospital (No. 2015-033). Informed consent was taken from all the patients.

References

1. Ettinger DS, Wood DE, Aisner DL, Akerley W, Bauman JR, Bharat A, et al. NCCN Guidelines Insights: Non-Small Cell Lung Cancer, Version 2.2021. J Natl Compr Canc Netw 2021;19:254-66.
2. Han S, Oh JS, Lee JJ. Diagnostic performance of deep learning models for detecting bone metastasis on whole-body bone scan in prostate cancer. Eur J Nucl Med Mol Imaging 2022;49:585-95.
3. Vičić I, Belev B. The pathogenesis of bone metastasis in solid tumors: a review. Croat Med J 2021;62:270-82.
4. Papandrianos N, Papageorgiou E, Anagnostis A, Papageorgiou K. Bone metastasis classification using whole body images from prostate cancer patients based on convolutional neural networks application. PLoS One 2020;15:e0237213.

5. Shan Q, Li Z, Lin J, Guo J, Han X, Song X, Wang H, Wang Z. Tumor Primary Location May Affect Metastasis Pattern for Patients with Stage IV NSCLC: A Population-Based Study. J Oncol 2020;2020:4784701.
6. Liu D, Kuai Y, Zhu R, Zhou C, Tao Y, Han W, Chen Q. Prognosis of prostate cancer and bone metastasis pattern of patients: a SEER-based study and a local hospital based study from China. Sci Rep 2020;10:9104.
7. Calin MA, Elfarra FG, Parasca SV. Object-oriented classification approach for bone metastasis mapping from whole-body bone scintigraphy. Phys Med 2021;84:141-8.
8. Kuo K, Kim AM. Rib Fracture. 2023.
9. Ma W, Quan Z, Wang J, Li X, Li G. The one-in-all diagnostic value of (99m)Tc-MDP bone scan combining with single-photon emission tomography (SPECT)/CT imaging in spinal osteoblastoma. J Orthop Surg Res 2020;15:181.
10. Clézardin P, Coleman R, Puppo M, Ottewell P, Bonnelye E, Paycha F, Confavreux CB, Holen I. Bone metastasis: mechanisms, therapies, and biomarkers. Physiol Rev 2021;101:797-855.
11. Zhuo L, Cheng Y, Pan Y, Zong J, Sun W, Xu L, Soriano-Gabarró M, Song Y, Lu J, Zhan S. Prostate cancer with bone metastasis in Beijing: an observational study of prevalence, hospital visits and treatment costs using data from an administrative claims database. BMJ Open 2019;9:e028214.
12. Li Q, Chen Z, Zhao Y, Li X, Pan H, Xia T, Chen L, Xu Z, Zhou W, Liu X. Risk of metastasis among rib abnormalities on bone scans in breast cancer patients. Sci Rep 2015;5:9587.
13. Qi N, Meng Q, You Z, Chen H, Shou Y, Zhao J. Standardized uptake values of (99m)Tc-MDP in normal vertebrae assessed using quantitative SPECT/CT for differentiation diagnosis of benign and malignant bone lesions. BMC Med Imaging 2021;21:39.

Cite this article as: Tong LQ, Jiang SN, Sui YF, Yin YH, Fu LQ, Zhong JY, Zhong JL. Imaging signs and the qualitative diagnosis of solitary rib lesions using 99mtechnetium-methylene diphosphonate whole-body bone imaging in patients with a malignant tumor. Quant Imaging Med Surg 2023;13(9):5688-5700. doi: 10.21037/qims-22-1159

